A mercury optical lattice clock at LNE-SYRTE

L. de Sarlo, M. Favier, R Tyumenev, S. Bize

A mercury optical lattice clock at LNE-SYRTE

Journal of Physics: Conference Series **723** (2016) 012017 doi:10.1088/1742-6596/723/1/012017

A mercury optical lattice clock at LNE-SYRTE

L De Sarlo, M Favier, R Tyumenev, S Bize

LNE-SYRTE, Observatoire de Paris, PSL Research University, CNRS, Sorbonne Universités, UPMC Univ. Paris 06, 61 avenue de l'Observatoire, 75014 Paris, France

E-mail: sebastien.bize@obspm.fr

Abstract. We describe the development of an optical lattice clock based on mercury and the results obtained since the 7^{th} SFSM. We briefly present a new solution for the cooling laser system and an improved lattice trap that allows us to interrogate a few thousand atoms in parallel. This translates into a fractional short term stability of 1.2×10^{-15} at the clock frequency of 1.129 PHz.

1. Introduction

Optical lattice clocks are based on the interrogation on a sample of cold atoms trapped in a laser standing wave at a suitable wavelength [1]. Thanks to the intrinsically low quantum projection noise associated to the interrogation of multiple particles, these devices are establishing themselves as a stability record breaking frequency standards. Leveraging on this unprecedented frequency stability, optical lattice clocks with an accuracy in the range of 10^{-18} are demonstrated in this conference and no limitation for their ultimate accuracy has been identified yet.

Among the atomic species employed in optical lattice clocks, mercury is particularly interesting because of a few remarkable properties. Mercury (Z=80) has an electronic structure dominated by two electrons in the 7s shell. This gives rise to a alkaline-earth-like structure, similar to that of Sr and Yb, the two other atomic species currently employed in optical lattice clocks. A level scheme of mercury is shown in the inset of figure 1.

Indeed, the clock transition in mercury has the same $^1S_0 \Rightarrow {}^3P_0$ character as in Sr and Yb. As in those atoms, the transition is strictly forbidden at zero magnetic field for bosonic isotopes (196,198,200,202) and only weakly allowed for the two fermionic isotopes (199,201) due to hyperfine mixing. The heavy atomic weight makes the $^1S_0 \Rightarrow {}^3P_1$ transition weakly allowed due to relativistic effects with a linewidth of around 1.2 MHz. This constitutes a first favorable property of mercury with respect to Sr and Yb in that such a linewidth allows for a simple laser cooling experimental scheme where atoms are directly loaded from the background pressure down to a temperature of about 30μK using a single MOT requiring only one laser source (see 3 below).

In addition to a level structure suitable for operating an optical lattice clock, mercury has an important advantage as far as the shift induced by thermal radiation is concerned. According to theoretical calculations of atomic static polarizabilities, the relative shift induced by thermal radiation at 300 K on the mercury clock transition is estimated to be -1.6×10^{-16} [2], 33 (16) times smaller than the corresponding shift for Sr (Yb). Note that the same scaling applies for differential DC Stark shift which can be introduced for instance by patch charges on the vacuum windows. A third advantage specific to the isotope ^{199}Hg is that, as ^{171}Yb but unlike ^{87}Sr, it

has a total spin of 1/2. This means that, by symmetry, the tensor component of the lattice light shift vanishes.

On a broader scope, mercury atom is of high interest for high precision atomic physics with application to fundamental physics tests including the search for variations of fundamental constants [3, 4, 5].

However, in order to exploit the full potential of the mercury atom, one challenge has to be overcome: all the required laser sources are in the deep UV part of the spectrum. Reliable and powerful laser sources at the wavelengths of 253.7 and 362.6 nm for respectively cooling and trapping, is therefore the main enabling technology for a mercury optical lattice clock.

In this paper we briefly describe the status of the mercury optical lattice clock at LNE-SYRTE first by recalling the results obtained in our group since the last Symposium on Frequency Standards and Metrology and then presenting the latest improvements on the experimental setup and on the performances of the clock.

2. Feasibility of a Hg optical lattice clock

At the 7$^{\text{th}}$ Symposium on Frequency Standards and Metrology, we reported some initial steps toward the operation of an optical lattice clock using mercury [6]. We reported the operation of a tandem of 2D and 3D magneto-optical trap, the implementation of a high performance clock laser system [7]. With these, we were able to perform the first laser spectroscopy of the clock transition on free-falling atoms released from the MOT. This yield absolute frequency measurements of the clock transition in ^{199}Hg and ^{201}Hg with accuracies of a few kHz [8]. Since then, we implemented a dipole lattice trap near the predicted magic wavelength and demonstrated optical trapping of mercury. We performed the first lattice-bound spectroscopy of the ^{199}Hg $^1S_0 - {}^3P_0$ optical clock transition and the first experimental determination of the ^{199}Hg magic wavelength : 362.5697 ± 0.0011 nm [9, 10]. Finally, we performed an absolute frequency measurement of the ^{199}Hg clock transition frequency using lattice trapped atoms obtaining a fractional uncertainty of 5.7×10^{-15} improving our previous measurement by 3 orders of magnitude [11, 12]. The obtained value of 1128 575 290 808 155.1 Hz $\pm$6.4(syst.) $\pm$ 0.3(stat) Hz is confirmed by the more accurate measurement reported three years later by the Katori's group [13]. This work clearly demonstrated the feasibility of a Hg lattice clock despite the considerable challenge due to deep UV laser sources.

3. An upgraded mercury lattice clock

After these first results we spent a significant amount of time improving the experimental setup in two critical subsystems: a new lattice trap allowing for a deeper lattice that will be described in Section 4 and a new cooling laser source that allows for a much more reliable operation of the clock that is described in the following. A detailed description of the other subsystems (e.g. vacuum system, clock laser) can be found in [7, 14]. A general overview of the mercury optical lattice clock setup is depicted in figure 1. Our new cooling laser source is based on a commercial fiber amplifier that amplifies the light of a custom-made extended cavity diode laser up to a power of around 12 W. This light is then frequency doubled in single-pass by focusing the output of the amplifier in a ppLN crystal and then further doubled by intracavity type I phase matching in a crystal of BBO enclosed in a bow-tie enhancement cavity.

The operating point of this second doubling stage requires a careful compromise between conversion efficiency and reliability. For an input power of 1.5 W at the wavelength of 508 nm the best efficiency we have achieved allows us in principle to obtain an output power of ~ 200 mW at 254 nm ($\eta \simeq 0.09\,\text{W}^{-1}$). As a matter of fact at this level of output power the operating lifetime of the BBO crystals is only a few days with maintainance operations required as often as every few hours. Experimentally we found out that decreasing the peak intracavity intensity at 508 nm to obtain only 70 mW of output power at 254 nm for an input power of 1.5 W ($\eta \simeq 0.03\,\text{W}^{-1}$),

increases the cooling laser uptime to a few weeks with crystal lifetimes typically exceeding several months. This level of power is enough to operate the MOT at the lowest observed temperatures ($30\,\mu$K) with a loading rate of about $\sim 1.3 \times 10^6$ atoms/s.

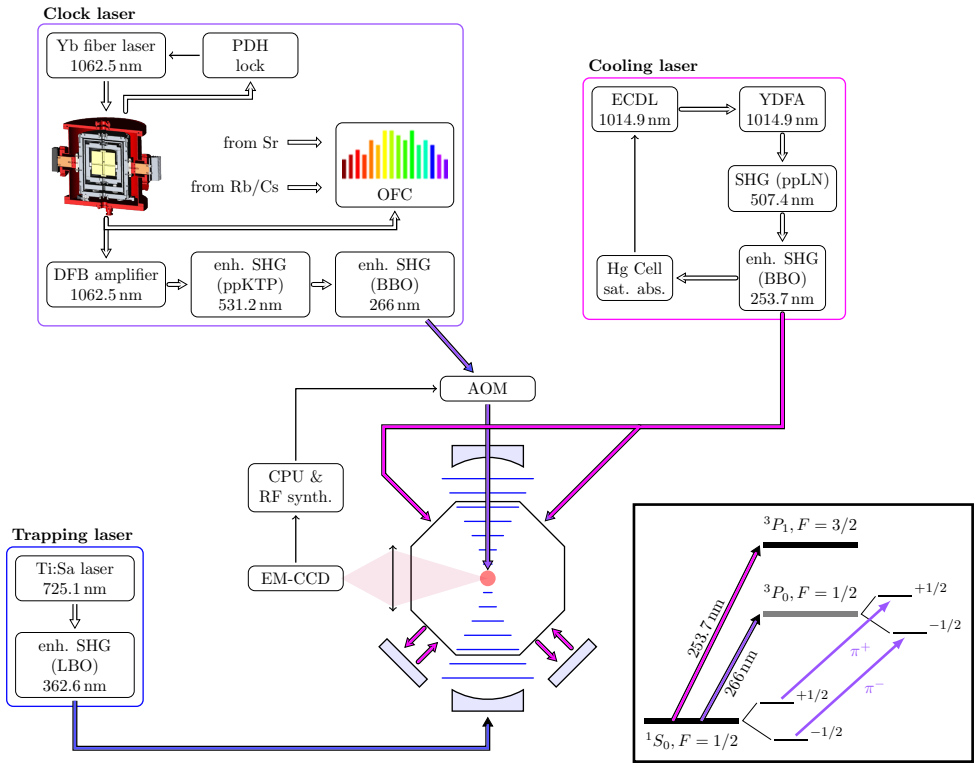

Figure 1: (Colour online) Schematics of the LNE-SYRTE's mercury optical lattice clock. One pair of MOT beams and the MOT coils are not shown. The inset shows a level scheme of mercury including the detail of the two Zeeman components of the clock transition.

4. A new lattice trap

The main limitation of the previous setup was the modest lattice trap depth of not more than 22 E_{rec}, where the recoil energy E_{rec} is the kinetic energy of a mercury atom with the momentum of a lattice photon. This limited trap depth gives poor collection efficiency of atoms from the MOT into the optical lattice (typically $> 0.5\%$) and limited confinement for the lattice-bound excitation of the clock transition [9]. The loading process is governed by two parameters: the trapping volume, and depth. Under the constraint of almost fixed laser power imposed by the damage threshold of the lattice optics a compromise shall be found between these two parameters in the form of an optimal value of the lattice beam waist [15]. Unfortunately this optimization is not easy on our experimental setup since the lattice standing wave is generated by a Fabry-Perot cavity whose mirror are also acting as vacuum windows (see figure 2a) and therefore changing the mirrors requires breaking the vacuum.

The initial size of the cavity mode was fixed based on estimation of the MOT size and temperature acquired in the earliest stage of the experiment. Based on the actual parameters of the MOT we decided to implement a new trap with a waist roughly two times smaller. This would maintain a good overlap between the MOT and the lattice while at the same time increasing the trap depth. Changing from a 250 mm radius of curvature to 150 mm, we decreased the waist from $120\,\mu$m to $69\,\mu$m expecting an improvement in the lattice depth by a factor of 3.

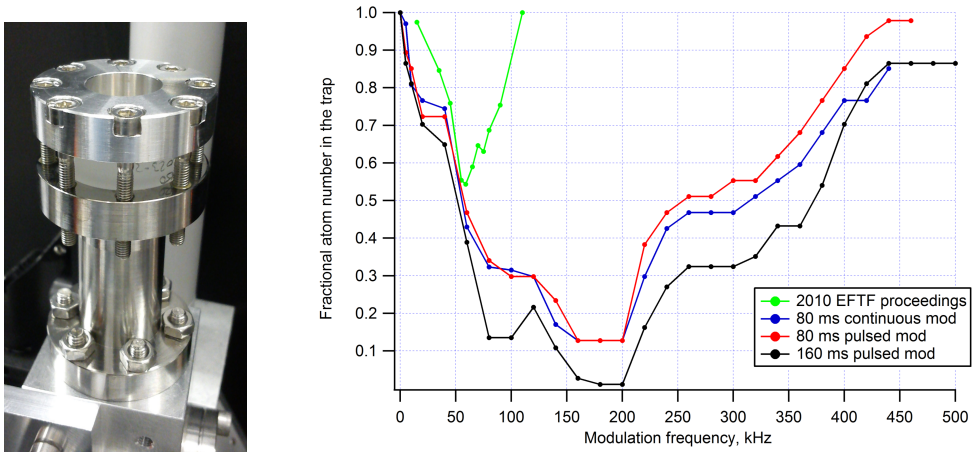

(a) (b)

Figure 2: (Colour online) *(a)* Picture of the new lattice mirrors mounted on the vacuum system. *(b)* Parametric excitation in the lattice.

Another improvement to the lattice subsystem was to servo the wavelength of the lattice to a commercial wavemeter with an accuracy of a few MHz. The wavemeter is periodically calibrated using the 698 nm clock light of SYRTE's Sr optical lattice clock.

In order to characterise atoms in the new trap we performed a parametric excitation experiment [16, 17, 18]. After loading atoms in the lattice, we modulate for a given time the power of the lattice at a frequency ν_m and observe the number of atoms remaining in the trap. When the parametric resonance condition $\nu_m = 2\nu_{\mathrm{trap}}$ is satisfied, the modulation excites the atomic sample inducing a loss of atoms. The results of the procedure are shown in figure 2b together with the results of the same procedure on the old lattice cavity normalized in such a way that the unperturbed signal is equal for the two curves. From the plots shown the increase in trapping oscillation frequency (and hence in lattice depth) is apparent: based on the peak at 180 kHz we infer a lattice depth of 56 recoils, consistent with the improvement expected from the waist reduction. We also observe a structure in the loss spectroscopy compatible with peaks at $\nu_{\mathrm{trap}} \simeq 90$ kHz, $3\nu_{\mathrm{trap}}$ and $4\nu_{\mathrm{trap}}$ that we tentatively attribute to the trapping anharmonicity and to the population distribution in the radial vibrational states. We emphasize that this topic definitely requires further investigation.

5. Improved spectroscopy and short term stability

The improvements detailed in the previous section allowed us to perform high resolution spectroscopy as shown in figure 3a. These data are obtained using the following typical experimental cycle. Starting from a mercury vapor at room temperature, we cool and trap $\sim 10^6$ ^{199}Hg atoms at a temperature of $\sim 30\,\mu$K in a 3D-MOT in the presence of the lattice light at a typical depth of $U \sim 56 E_{\mathrm{rec}} \simeq h \times 0.43$ MHz $\simeq k_B \times 20\,\mu$K. Following a compressed MOT phase the cooling light is turned off leaving the atoms in the lattice. The overall capture efficiency is around 2%, improved by a factor 10 with respect to the previous configuration, but still limited by the fraction of MOT atoms having an energy below the lattice depth. The typical duration of this capture phase is about 0.7 s.

Before applying a standard rectangular Rabi pulse, we perform initial state selection with a simple procedure that consist in two light pulses. A first short (15 ms) π-pulse of clock light tuned to the Zeeman component that is to be selected, transfers roughly half of all atoms to the

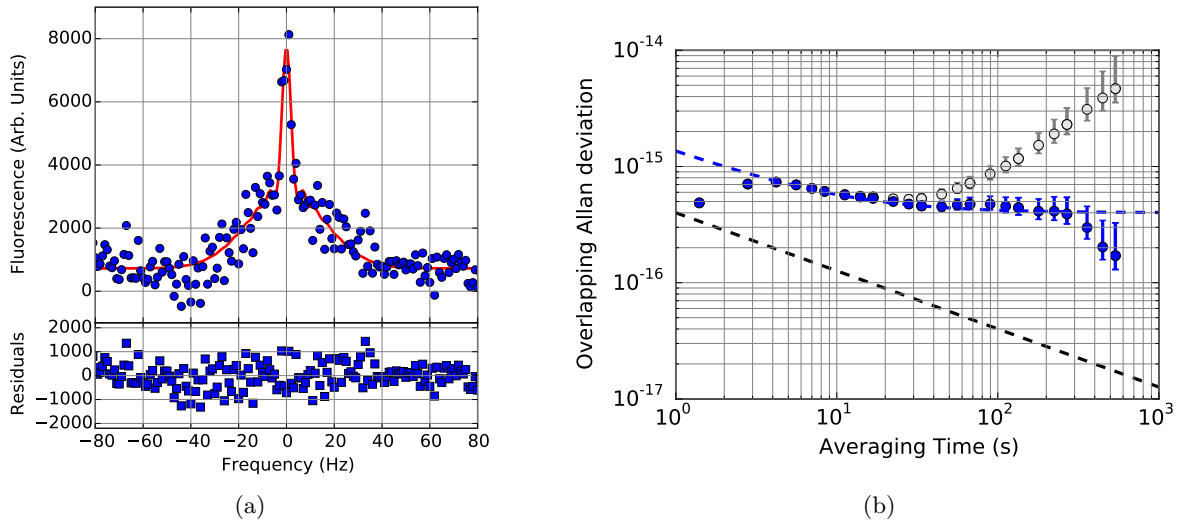

(a) (b)

Figure 3: (Colour online) *(a)* Typical spectroscopy signal for one of the π components of the ^{199}Hg clock transition. Here Rabi time is 0.2 s and the fit function is the sum of a Rabi profile (fitted width 4.2 Hz) on a gaussian background. *(b)* Overlapping Allan deviation of the fractional frequency difference between the mercury clock laser and the mercury clock transition at 1.128 PHz in a closed integrator loop (gray) and dedrifted data (blue). Noise is modeled as the sum of the white noise of the clock and the flicker of the cavity (blue dashed line). The black dashed line corresponds to the Dick limit for short term stability.

excited clock state. A second pulse of light resonant with the cooling transition then removes atoms that are left in the ground state.

Following this procedure we perform spectroscopy on the clock transition by applying a Rabi pulse that is tuned to transfer at resonance all the atoms from the excited clock state to the ground state. We then detect the transferred atoms by collecting fluorescence of $^1S_0$ atoms from a molasses made by the four MOT beams depicted in figure 1, slightly ($\sim$ 2MHz $\sim 1.5\Gamma$) detuned from the cooling resonance.

The data shown in the figure 3a are taken for a Rabi time of 0.2 s. The fit to a Rabi model is consistent with the expected linewidth of 4.2 Hz and a gaussian background attributed to the flicker noise of the clock laser [19]. Note that, since the clock frequency is 1.13 PHz, this corresponds to an atomic quality factor of $Q \simeq 3.7 \times 10^{14}$ roughly the same as in the Sr case for a linewidth of 1.7 Hz. The peak signal to noise ratio is about 15.

When we operate in clock mode, we use the collected fluorescence to correct the frequency of the clock laser at each cycle. The equivalent detection noise is about 40 atoms but the spectroscopic signal to noise ratio is limited by shot to shot fluctuations in the total atom number typically one order of magnitude bigger. We note that we plan to negate the effect of this kind of fluctuations on the frequency discrimination by introducing a normalized detection.

We plot the overlapping Allan deviation of the relative frequency difference between the mercury clock laser and the mercury clock transition in a closed integrator loop in figure 3b for the typical Rabi time of 0.1 s. As we can see the data are well reproduced by a noise model comprising three terms : white frequency noise determined by the atomic resonator for averaging times between 2 and 8 seconds, flicker noise in frequency corresponding to the noise floor of our clock laser between 10 and 30 seconds, and finally a residual uncompensated frequency drift for longer averaging times.

By adjusting these noise form to the data we are able to infer the short term stability of our

atomic frequency discriminator which is $1.2(1) \times 10^{-15}$ at 1s (almost a factor 5 improvement over our previous value [20]) and the noise floor of our clock laser which is $3.5(5) \times 10^{-16}$, in good agreement with the value inferred from the comparison of two similar laser [7]. As shown in figure 3b, the estimated stability limit from the Dick effect, as obtained from the parameters of reference [7], is significantly lower. Stabilities in the mid 10^{-16} range will be within reach when the detection noise will be lowered.

6. Latest developments and outlook

With the improvements reported in previous sections, we are characterizing systematic frequency shifts of the ^{199}Hg optical lattice clocks with individual uncertainties in the 10^{-17} range. Once completed, this work will allow us to perform optical to optical frequency ratio measurements against SYRTE's Sr lattice clocks [21] and to compared the result with the recent value of [13]. It will also yield refined measurements against Cs (and Rb) fountain clocks [22].

One of the advantages of Hg is the possibility to implement and use a high flux cold atom source based on a 2D-MOT loaded from thermal vapor. This possibility was so far underexploited due to the difficulty to obtain reliable laser sources at the cooling wavelength of 254 nm. The advent of fiber-based laser technology for this source which was described in section 3 has removed this obstacle. In the future, we hope to exploit this possibility to obtain stabilities at the 1×10^{-16} level at one second and to explore the limits of Hg optical lattice clocks which we expect to be below 1×10^{-18}.

Acknowledgments

We acknowledge the large number of contributions of SYRTE technical services. This work was supported by EMRP/JRP ITOC and by ERC Consolidator Grant AdOC. We acknowledge funding support from Centre National d'Études Spatiales (CNES), Conseil Régional Île-de-France (DIM Nano'K).

References

[1] Katori H, Takamoto M, Pal'Chikov V G and Ovsiannikov V D 2003 *Physical Review Letters* **91** 173005
[2] Hachisu H, Miyagishi K, Porsev S G, Derevianko A, Ovsiannikov V D, Pal'chikov V G, Takamoto M and Katori H 2008 *Phys. Rev. Lett.* **100**(5) 053001
[3] Angstmann E J, Dzuba V A and Flambaum V V 2004 *Phys. Rev. A* **70** 014102
[4] Tobar M E, Stanwix P L, McFerran J J, Guéna J, Abgrall M, Bize S, Clairon A, Laurent P, Rosenbusch P, Rovera D and Santarelli G 2013 *Phys. Rev. D* **87**(12) 122004
[5] Huntemann N, Lipphardt B, Tamm C, Gerginov V, Weyers S and Peik E 2014 *Phys. Rev. Lett.* **113**(21) 210802
[6] Petersen M, Millo J, Magalhaes D V, Mandache C, Dawkins S T, Chicireanu R, Lecoq Y, Guena J, Chapelet F, Rosenbusch P, Laurent P, Abgrall M, Rovera G D, Santarelli G, Clairon A, Bize S and Tobar M E 2009 *PROCEEDINGS OF THE 7TH SYMPOSIUM FREQUENCY STANDARDS AND METROLOGY* ed Maleki, L (WORLD SCIENTIFIC PUBL) pp 82–90
[7] Dawkins S T, Chicireanu R, Petersen M, Millo J, Magalhães D V, Mandache C, Le Coq Y and Bize S 2010 *Applied Physics B: Lasers and Optics* **99** 41–46
[8] Petersen M, Chicireanu R, Dawkins S T, Magalhães D V, Mandache C, Le Coq Y, Clairon A and Bize S 2008 *Physical Review Letters* **101** 183004 (*Preprint* `0807.3408`)
[9] Yi L, Mejri S, McFerran J J, Le Coq Y and Bize S 2011 *Phys. Rev. Lett.* **106** 073005
[10] Mejri S, McFerran J J, Yi L, Le Coq Y and Bize S 2011 *Phys. Rev. A* **84** 032507
[11] McFerran J J, Yi L, Mejri S, Di Manno S, Zhang W, Guéna J, Le Coq Y and Bize S 2012 *Phys. Rev. Lett.* **108**(18) 183004
[12] McFerran J J, Yi L, Mejri S, Di Manno S, Zhang W, Guéna J, Le Coq Y and Bize S 2015 *Phys. Rev. Lett.* **115**(21) 219901
[13] Yamanaka K, Ohmae N, Ushijima I, Takamoto M and Katori H 2015 *Physical Review Letters* **114** 230801
[14] McFerran J J, Yi L, Mejri S, Zhang W, Di Manno S, Abgrall M, Guéna J, Le Coq Y and Bize S 2014 *Phys. Rev. A* **89**(4) 043432
[15] Kuppens S J M, Corwin K L, Miller K W, Chupp T E and Wieman C E 2000 *Phys. Rev. A* **62**(1) 013406

[16] Gehm M E, O'Hara K M, Savard T A and Thomas J E 1998 *Phys. Rev. A* **58**(5) 3914–3921
[17] Gehm M E, O'Hara K M, Savard T A and Thomas J E 2000 *Phys. Rev. A* **61**(2) 029902
[18] Wu J, Newell R, Hausmann M, Vieira D J and Zhao X 2006 *Journal of Applied Physics* **100** 054903
[19] Di Domenico G, Schilt S and Thomann P 2010 *Appl. Opt.* **49** 4801–4807
[20] McFerran J J, Magalhaes D V, Mandache C, Millo J, Zhang W, Le Coq Y, Santarelli G and Bize S 2012 *OPTICS LETTERS* **37** 3477–3479
[21] Le Targat R, Lorini L, Le Coq Y, Zawada M, Guéna J, Abgrall M, Gurov M, Rosenbusch P, Rovera D G, Nagórny B, Gartman R, Westergaard P G, Tobar M E, Lours M, Santarelli G, Clairon A, Bize S, Laurent P, Lemonde P and Lodewyck J 2013 *Nature Communications* **4** 2109 (*Preprint* `1301.6046`)
[22] Guena J, Abgrall M, Rovera D, Laurent P, Chupin B, Lours M, Santarelli G, Rosenbusch P, Tobar M, Li R, Gibble K, Clairon A and Bize S 2012 *Ultrasonics, Ferroelectrics, and Frequency Control, IEEE Transactions on* **59** 391–409 ISSN 0885-3010